International Journal of Minerals, Metallurgy and Materials
Volume 27, Number 5, May 2020, Page 649
https://doi.org/10.1007/s12613-019-1943-1

Comparative studies on the hot corrosion behavior of air plasma spray and high velocity oxygen fuel coated Co-based L605 superalloys in a gas turbine environment

Kuzhipadath Jithesh[1)] *and Moganraj Arivarasu*[2)]

1) School of Mechanical Engineering, Vellore Institute of Technology, Vellore, Tamilnadu-632014, India
2) Center for Innovative Manufacturing Research, Vellore Institute of Technology, Vellore, Tamilnadu-632014, India
(Received: 14 September 2019; revised: 13 November 2019; accepted: 20 November 2019)

Abstract: An improvement in the corrosion resistance of alloys at elevated temperature is a factor for their potential use in gas turbines. In this study, CoNiCrAlY has been coated on the L605 alloy using air plasma spray (APS) and high-velocity oxygen fuel (HVOF) coating techniques to enhance its corrosion resistance. Hot corrosion studies were conducted on uncoated and coated samples in a molten salt environment at 850°C under cyclic conditions. Thermogravimetric analysis was used to determine the corrosion kinetics. The samples were subjected to scanning electron microscopy, energy-dispersive spectroscopy, and X-ray diffraction for further investigation. In coated samples, the formation of Al_2O_3 and Cr_2O_3 in the coating acts as a diffusion barrier that could resists the inward movement of the corrosive species present in the molten salt. Coated samples showed very less spallation, lower weight gain, less porosity, and internal oxidation as compared to uncoated sample. HVOF-coated sample showed greater corrosion resistance and inferred that this is the best technique under these conditions.

Keywords: L605 alloy; hot corrosion; air plasma spray; high velocity oxygen fuel; cross-sectional analysis

1. Introduction

The advancement of superalloys in terms of their performances and properties will be a significant factor in the development of power generation sectors, such as for gas turbines and boilers [1−3]. In this field, various types of fuels, such as low-grade fuel oils and fossil fuels are used for power generation applications. The major impurities present in these fuels contain sodium, chlorine, sulfur, and vanadium, which when subjected to high temperature during operation, will turn to complex compounds, such as sodium sulfate (Na_2SO_4), sodium chloride (NaCl), sodium metavanadate ($NaVO_3$), and vanadium pentoxide (V_2O_5) [4−7]. These thin films of molten salt compounds on the substrate surface of components will produce unsafe oxide layers, which can cause severe deterioration. This phenomenon of accelerated corrosion is called hot corrosion [8]. Owing to this hot corrosion, the superalloys used in this field, although selected for its excellent mechanical properties, fail to perform when subjected to long-term elevated temperature.

Several coating methods and coating powders are available to provide desirable specifications for each application area. The thermal spray coating technique is a surface modification method that is one of the better options because it provides an economical way to protect the surface from hot corrosion without altering the mechanical properties of the substrate metal [9]. Air plasma spray (APS) and high velocity oxygen fuel (HVOF) are the two types of thermal spray coating methods used to deposit cobalt-based coating powder on the surface of substrate materials [10−13]. MCrAlY, where M could be cobalt, nickel, or a combination of cobalt and nickel, is widely used to develop various thicknesses from several micrometers to tenths of a millimeter on the substrate material.

Jegadeeswaran *et al*. [4] investigated the hot corrosion behavior of the cobalt-based superalloy, super-605, in the presence of Na_2SO_4 + 50wt% V_2O_5 at 800°C. They reported extensive spalling on the substrate surface and suggested that a 10wt% Al_2O_3 + 90wt% CoCrAlTaY coating made by the HVOF process improved the corrosion resistance of super-605. Mangla *et al*. [14] published a comparison of hot corrosion behavior on Ni20Cr-coated T-22 steel by the HVOF and APS methods in an actual coal-fired boiler environment at 700°C. The results showed that the HVOF-coated sample

Corresponding author: Moganraj Arivarasu E-mail: arivarasu.m@vit.ac.in; arivarasu.m@gmail.com

had better corrosion resistance. In the available literature, no reports of a comparative study of the APS- and HVOF-coated L605 alloy in a simulated gas turbine environment. A detailed cross-sectional analysis of the two different coating techniques will add value to the literature.

This investigation compared the hot corrosion behavior of CoNiCrAlY powder coated using the two thermal spray processes, APS and HVOF, on the cobalt-based superalloy, L605. Hot corrosion tests of coated and bare specimens were performed, and the results were analyzed via thermogravimetric analysis, scanning electron microscopy (SEM), energy-dispersive spectroscopy (EDS), and X-ray diffraction (XRD).

2. Experimental

2.1. Substrate material and sample preparation

The cobalt-based superalloy, L605 (also known as Haynes 25), was used as a substrate material for this study. The material was bought in plate form and was supplied by Vikas Metals, Secunderabad, India. The chemical composition analysis of the L605 alloy was conducted via optical emission spectroscopy. The actual chemical composition of the L605 alloy is listed in Table 1. Three specimens with dimensions of 20 mm × 10 mm × 7 mm were cut from the plate using wire electrical discharge machining (WEDM) for the analysis. The specimens were polished using silicon carbide papers of various standard sizes to achieve a mirror finish and were grit blasted with alumina powders of 300−350 μm before the coating processes to improve the adhesion characteristics of the substrate surface.

Table 1. Chemical composition of the L605 alloy wt%

Ni	Cr	W	Fe	Mn	Si	C	Mo	Co
10.91	20.39	14.78	0.35	1.45	0.13	0.048	0.038	51.904

2.2. Coating characterization

The coating material used for this analysis was a gas-atomized CoNiCrAlY powder with a spheroidal morphology. It consists of 32wt% Ni, 21wt% Cr, 8wt% Al, 0.5wt% Y, and a balance of Co. Thermal spray coating techniques, such as APS and HVOF coatings, were the two primary coating techniques considered for this investigation owing to their lower environmental impact and low application cost [15]. The process parameters used for the APS and HVOF coatings are presented in Tables 2 and 3, respectively. Both coating processes were carried out at Spraymet Surface Technologies, Bangalore.

2.3. Hardness measurement

The microhardness test was conducted using a Vickers microhardness tester on the polished cross sections of the APS- and HVOF-coated samples. During the test, a load/force of 0.5 N was applied on the sample for 10 s of dwell time with a distance of 60 μm between each indentation. The indentation was performed at five different locations on each sample, and an averaged hardness value was recorded.

Table 2. Process parameters used for APS coating

Parameters	Value
Voltage / V	60−65
Current / A	400
Argon pressure / (10^5 N·m^{-2})	7
Argon flow rate / (m^3·s^{-1})	0.00083
Hydrogen pressure / (10^5 N·m^{-2})	4
Hydrogen flow rate / (m^3·s^{-1})	0.00007
Powder feed rate / (kg·s^{-1})	0.0018
Spray distance / m	0.1−0.15

Table 3. Process parameters used for HVOF coating

Parameters	Value
Nozzle type	DJH 2603
Oxygen pressure / (10^5 N·m^{-2})	12
Oxygen flow rate / (m^3·s^{-1})	0.0043
Fuel flow rate / (m^3·s^{-1})	0.001−0.00117
Hydrogen pressure / (10^5 N·m^{-2})	9
Powder feed rate / (kg·s^{-1})	0.0015
Spray distance / m	0.2−0.25

2.4. Hot corrosion studies

Uncoated, APS-coated, and HVOF-coated samples of the L605 alloy were used for the comparative study on hot corrosion. To duplicate an environment similar to the application sectors that use superalloys, such as aerospace, marine, and power generation sectors, a molten salt of 87.5wt% Na_2SO_4 + 7.5wt% $NaVO_3$ + 5wt% NaCl was created to apply on the sample [16−17]. The coated and uncoated specimens were uniformly covered by molten salt using a camel wire brush with a coverage area of 3–5 mg/cm^2. Each specimen was kept in an alumina boat, and the weight of the boat and sample was measured using an electronic weight balance before and after the application of molten salt on the specimen. Before beginning the heating and cooling cycles, the sample was preheated for 2 h in a furnace at 120°C to remove moisture. Subsequently, the hot corrosion test was conducted in a tubular furnace at 850°C for 50 cycles, and the samples were monitored during each cycle. Each cycle consisted of 1 hour of heating followed by 20 minutes of air cooling. The corrosion products that spalled during the hot corrosion were included in the weight change measurements. Visual observations and weight changes were monitored and recorded at the end of each cycle. The weight gain/loss and corrosion rate were analyzed to determine the corrosion resistance of the samples. The hot-corroded sample surfaces and cross sections were analyzed via SEM/EDS, EDS line mapping analysis, and XRD to identify the corrosion products.

3. Results

3.1. Characterization of the coated samples

The SEM images in Fig. 1 show the cross sections, i.e., the cut section of the coated substrate perpendicular to the coated surface by using WEDM, of the APS- and HVOF-coated samples. In both samples, the coating properly adhered to the substrate surface. The average thicknesses of the APS and HVOF coatings were 230 and 245 μm, respectively.

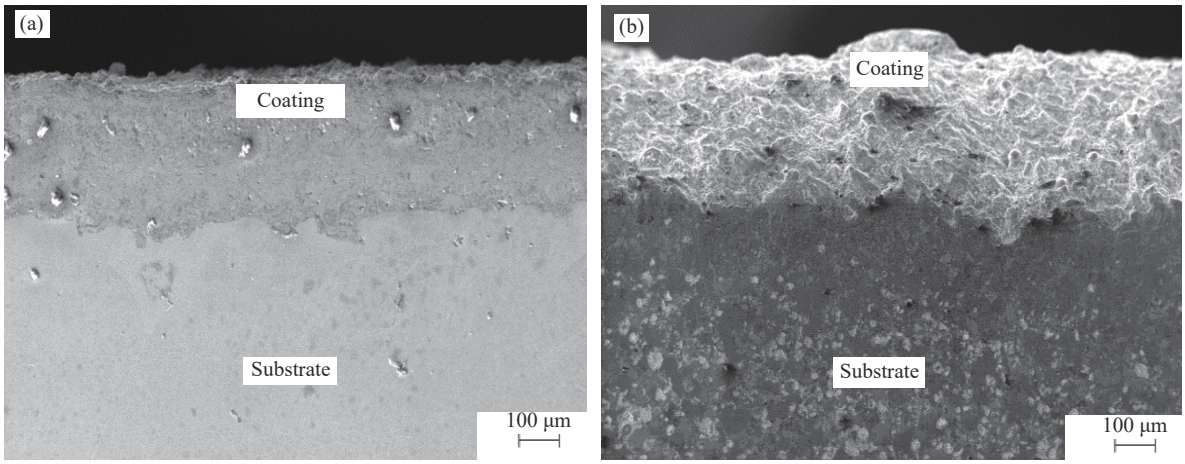

Fig. 1. Cross section SEM images of the L605 alloys coated by different coating processes: (a) APS coating; (b) HVOF coating.

3.2. Microhardness

Fig. 2 shows the microhardness profile of the APS- and HVOF-coated samples. The hardness at the substrate, interface, and coating was found for each sample. Average hardness values of HV 590 for the APS-coated sample, HV 791 for the HVOF-coated sample, and HV 279 for the substrate were obtained. The APS- and HVOF-coated samples showed a 112% and 184% increased hardness compared to the substrate surface, respectively.

3.3. Visual inspection and thermogravimetric studies

Figs. 3–5 show the optical micrographs of the coated and uncoated samples at various stages of the hot corrosion. In the uncoated sample, spalling and sputtering started from 1st cycle. The effects were visible when the glossy color changed to dark grey along with cracks on the surface. During the hot corrosion, the scales started to separate from the substrate surface, which became severe from the 5th cycle onwards. Meanwhile, the samples that were coated with CoNiCrAlY powder by APS and HVOF showed fewer cracks and had a dark gray color. The cross-sectional optical microscopy images shown in Fig. 6 confirmed that the HVOF-coated sample had minor porosity and interfacial cracks compared to the APS-coated sample.

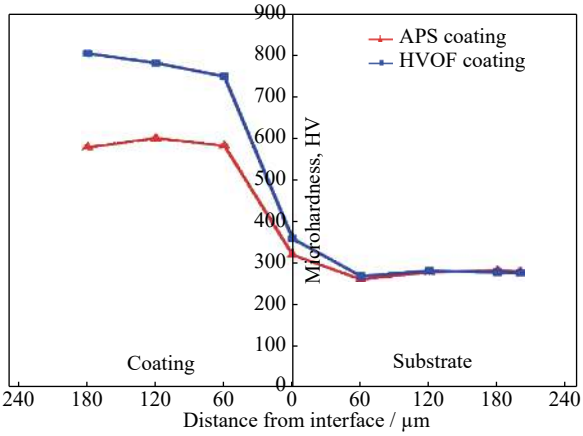

Fig. 2. Microhardness profile of the APS- and HVOF-coated samples.

The thermogravimetric analysis of the samples was performed to investigate the weight gain per unit area (mg/cm^2) as a function of time in hours. The results are illustrated in Fig. 7. All three samples showed weight gain from the 1st cycle onwards. The uncoated sample showed aggressive weight gain during the entire cycle, which indicated oxide formation on the surface. The cumulative weight gain was 4.87 mg/cm^2. The APS-coated sample showed weight gain up to the 4th cycle, after which the weight began to decrease. At the end of the 8th cycle, a severe decline in the weight gain was observed, which may have been due to sputtering caused by the stresses induced by thermal expansion and contraction. Afterwards, no more weight changes were observed. The cumulative weight gain for the APS-coated sample after the hot corrosion test was 1.25 mg/cm^2. The experiment on the HVOF-coated sample showed a weight gain up to 4th cycle; then, the weight gain started to decrease similar as for the APS-coated sample. Here, the sample demonstrated an accumulative weight gain of 0.695 mg/cm^2. The parabolic rate constant, K_p, was calculated by $(\Delta W/A)^2 = (K_p$

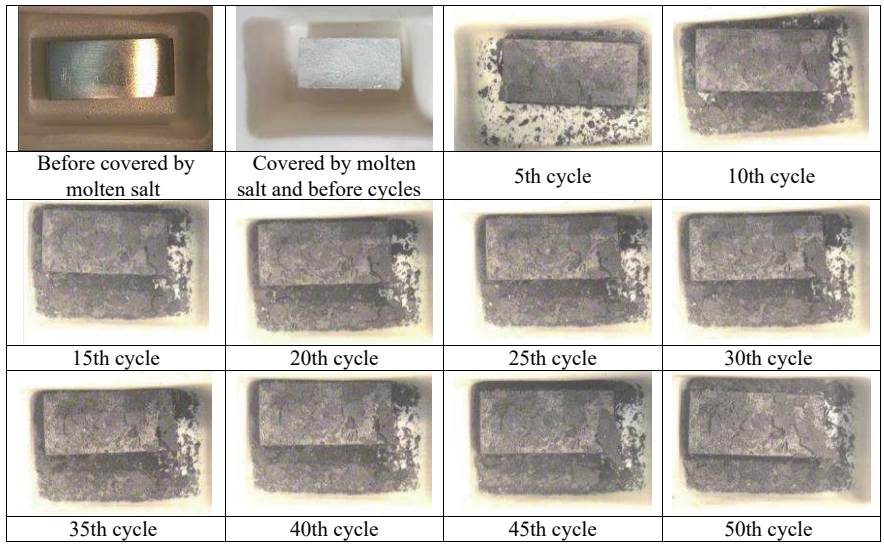

Fig. 3. Macro images of the hot corrosion behavior of the uncoated sample at various cycles.

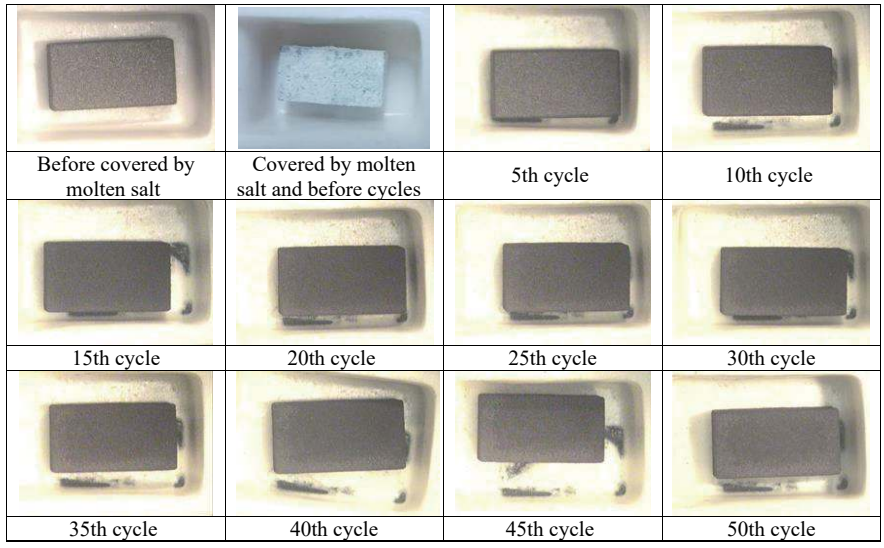

Fig. 4. Macro images of the hot corrosion behavior of the APS-coated sample at various cycles.

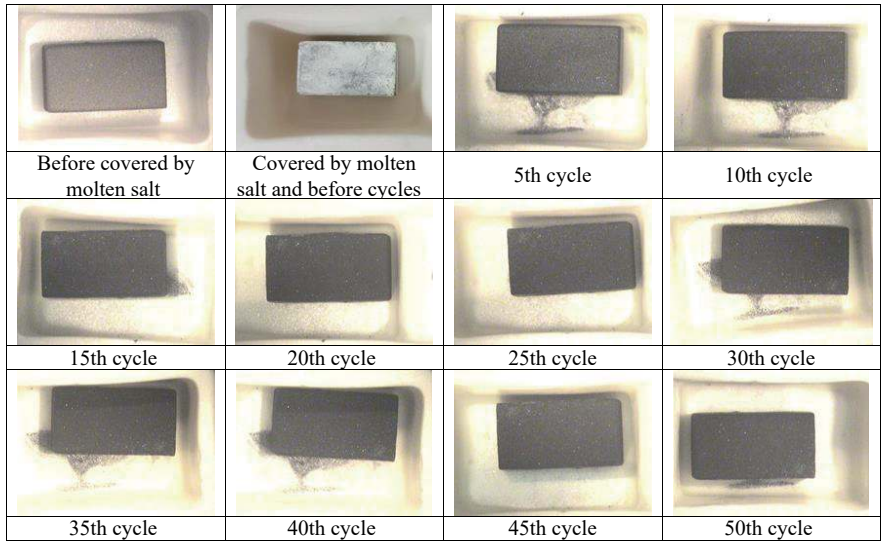

Fig. 5. Macro images of the hot corrosion behavior of the HVOF-coated sample at various cycles.

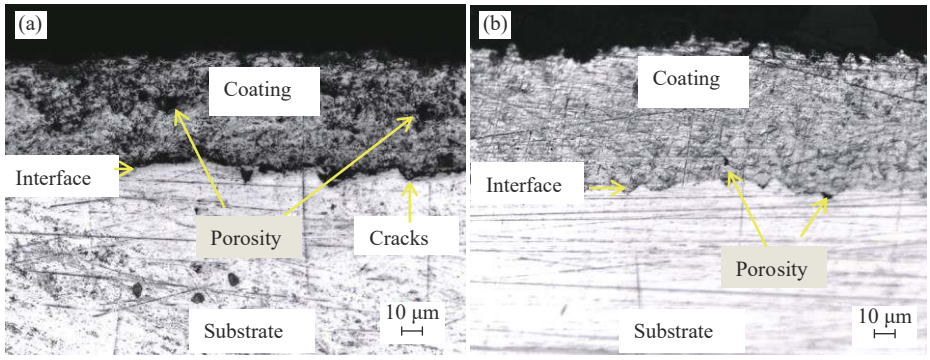

Fig. 6. Cross-sectional optical microscopy images of L605 alloy after the 50th cycle of hot corrosion: (a) APS-coated; (b) HVOF-coated.

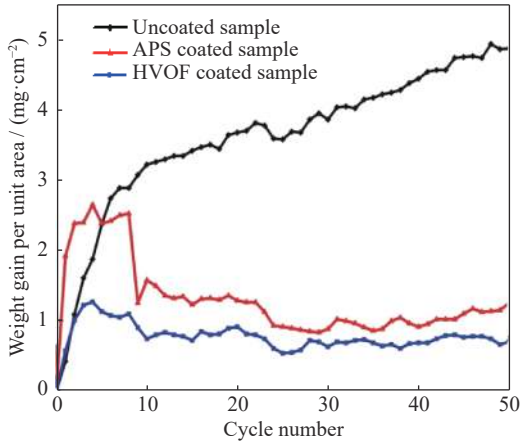

Fig. 7. Weight gain per unit area vs. cycle number for uncoated, APS-coated, and HVOF-coated samples subject to hot corrosion in the 87.5wt% Na_2SO_4 + 7.5wt% $NaVO_3$ + 5wt% NaCl molten salt at 850°C.

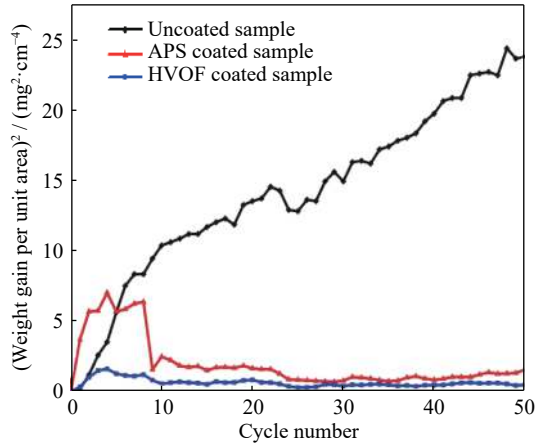

Fig. 8. (Weight gain per unit area)^2 vs. cycle number for uncoated, APS-coated, and HVOF-coated samples subjected to hot corrosion in the 87.5wt% Na_2SO_4 + 7.5wt% $NaVO_3$ + 5wt% NaCl molten salt at 850°C.

× t), where $\Delta W/A$ represents the weight gain per unit area (mg/cm^2), and t represents the hot corrosion time in seconds. To obtain the corrosion kinetics, a graph of the number of cycles vs. $(\Delta W/A)^2$ was plotted, which is shown in Fig. 8. The parabolic rate constants (K_p) for the uncoated, APS-coated, and HVOF-coated samples after 50 cycles of hot corrosion were calculated as 1319 × 10^{-10}, 86.71 × 10^{-10}, and 26.83 × 10^{-10} g^2·cm^{-4}·s^{-1}, respectively. Thus, the uncoated sample showed a maximum weight gain during hot corrosion compared to the coated samples, but further investigation also revealed that the HVOF-coated sample showed less weight gain in contrast with the APS-coated sample, making it the better coating technique.

3.4. SEM/EDS analysis

Figs. 9–11 shows the SEM images and EDS analysis of the uncoated and coated samples of the L605 alloy after 50 cycles of exposure to the 87.5wt% Na_2SO_4 + 7.5wt% $NaVO_3$ + 5wt% NaCl molten salt at 850°C. Fig. 9 shows the formation of an oxide layer on the surface of the uncoated sample. The oxide scales formed were irregular shapes and had various sizes, which were accompanied by cracks leading to non-adhesion on the surface. The surface morphology of the uncoated sample showed intensive spalling of the oxide scale that formed, which are observable in the macro images in Fig. 3. The EDS analysis of the selected area on the uncoated samples showed a significant amount of oxygen with moderate amounts of chromium, tungsten, sodium, and cobalt.

As shown in the Fig. 10, the surface morphology of the APS-coated sample showed oxide scales with irregular shapes and sizes. Some massive structures were visible that contained large clusters. In the EDS analysis of the selected area on the APS-coated sample, oxide layers of chromium, nickel, and cobalt were present. Fig. 11 shows that the HVOF-coated sample had oxide scales with an uneven surface, which were appropriately adherent to the substrate surface, showing very little porosity. The EDS analysis of the selected area on the HVOF coating showed oxide layers of chromium, aluminum, nickel, and cobalt.

3.5. EDS line mapping analysis

The line mapping analysis of the cross section of the un-

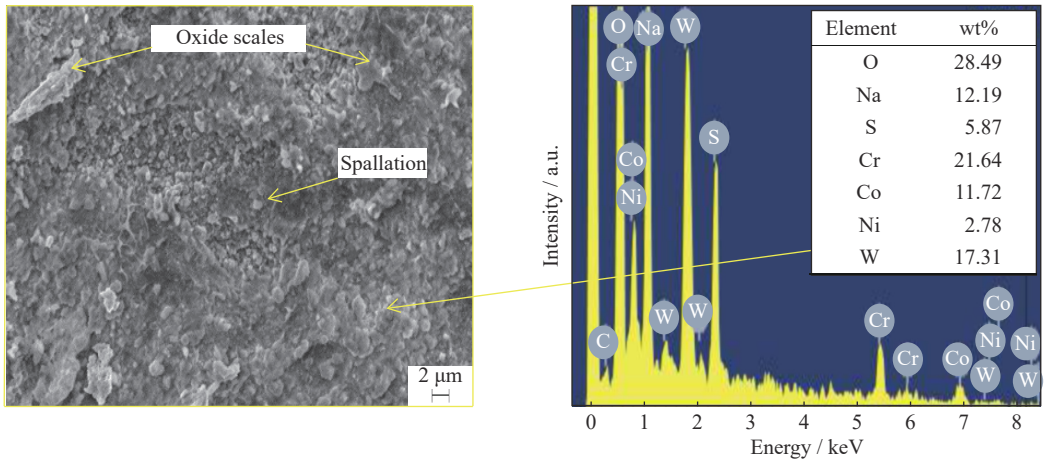

Fig. 9. SEM/EDS analysis of the uncoated L605 alloy subjected to hot corrosion in the 87.5wt% Na_2SO_4 + 7.5wt% $NaVO_3$ + 5wt% NaCl molten salt at 850°C for 50 cycles.

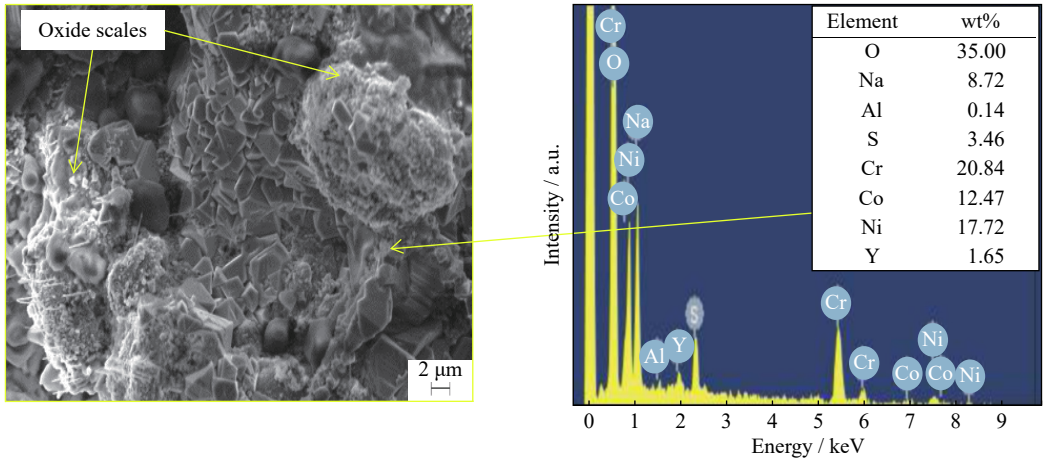

Fig. 10. SEM/EDS analysis of the APS-coated L605 alloy subjected to hot corrosion in the 87.5wt% Na_2SO_4 + 7.5wt% $NaVO_3$ + 5wt% NaCl molten salt at 850°C for 50 cycles.

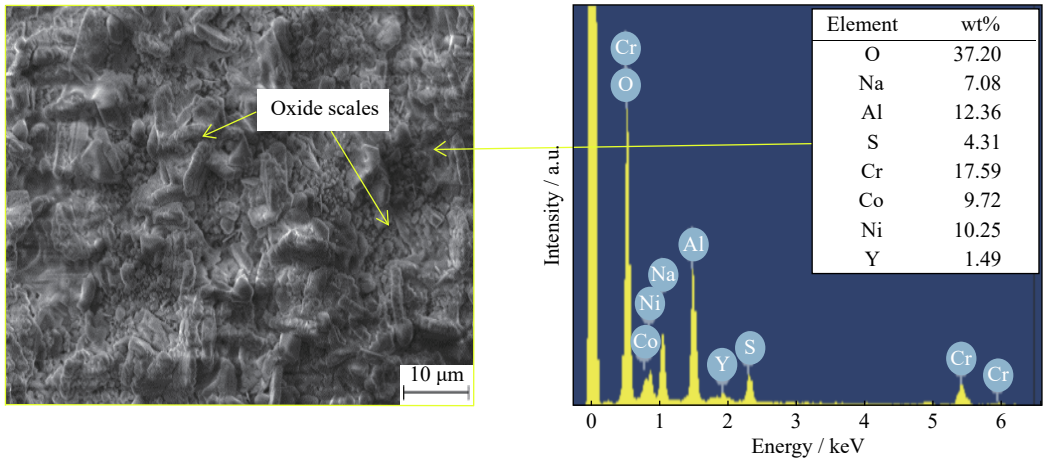

Fig. 11. SEM/EDS analysis of the HVOF-coated L605 alloy subjected to hot corrosion in the 87.5wt% Na_2SO_4 + 7.5wt% $NaVO_3$ + 5wt% NaCl molten salt at 850°C for 50 cycles.

coated, APS-coated, and HVOF-coated samples after hot-corroded is shown in Figs. 12–14 with the formation of oxides on the surface. The presence of excess oxygen in the outer layer of the oxide was confirmed in all three samples via the line mapping, and the uncoated sample showed the presence of tungsten in the top layer, whereas the inner layer con-

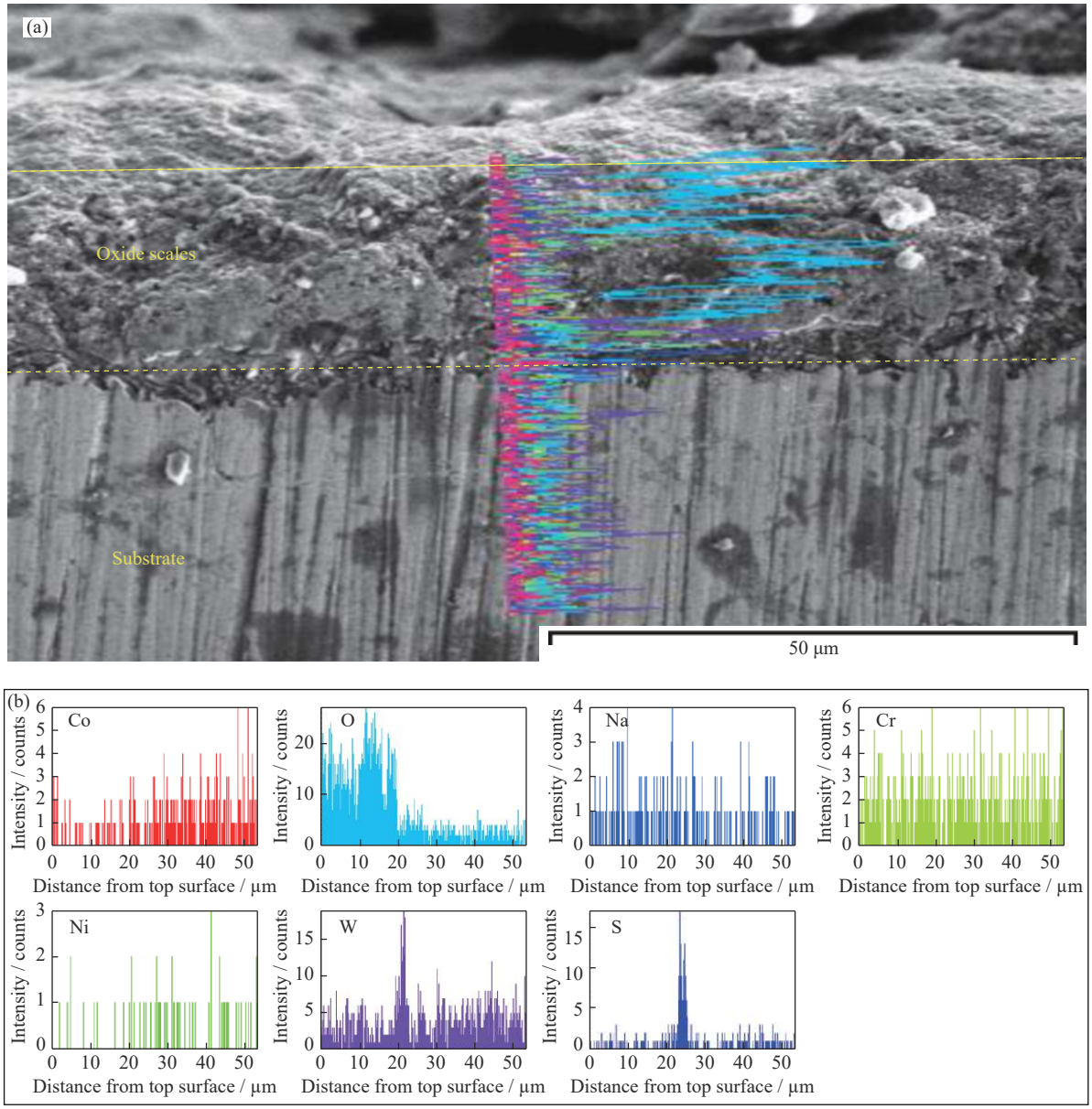

Fig. 12. Line mapping analysis for the cross section of the uncoated L605 alloy subjected to hot corrosion after 50 cycles at 850°C: (a) mapping direction; (b) distribution of different elements.

sisted of chromium and cobalt. In the APS-coated sample, the top layer was rich in chromium, and the inner layer consisted of nickel and cobalt; however, in the HVOF-coated sample, the top layer was rich in chromium, and the inner layer consisted of aluminum, nickel, and cobalt.

3.6. XRD analysis

In Fig. 15, the XRD data are plotted for the 87.5wt% Na_2SO_4 + 7.5wt% $NaVO_3$ + 5wt% NaCl hot corroded samples for the uncoated (substrate), APS-coated, and HVOF-coated samples. Here, the uncoated sample showed the formation of WO_3, $Na_2Cr_2O_7$, and FeO_2 as the components in the scale. The XRD data for the APS-coated sample after the 50th cycle of hot corrosion revealed Al_2O_3, Cr_2O_3, $CoAl_2O_4$, and $NiCr_2O_4$ as the prominent phases that formed. The XRD data for the HVOF-coated sample after the 50th cycle of hot corrosion revealed Al_2O_3, Cr_2O_3, and $CoAl_2O_4$ as the prominent phases that formed.

4. Discussion

Successful coatings of CoNiCrAlY powder on the L605 alloy were performed via the APS and HVOF coating methods. Then, these samples were subjected to hot corrosion in the 87.5wt% Na_2SO_4 + 7.5wt% $NaVO_3$ + 5wt% NaCl molten salt environment for 50 cycles at 850°C. Upon visual inspection, the coated samples showed much less spallation compared to the uncoated samples at various stages of the hot

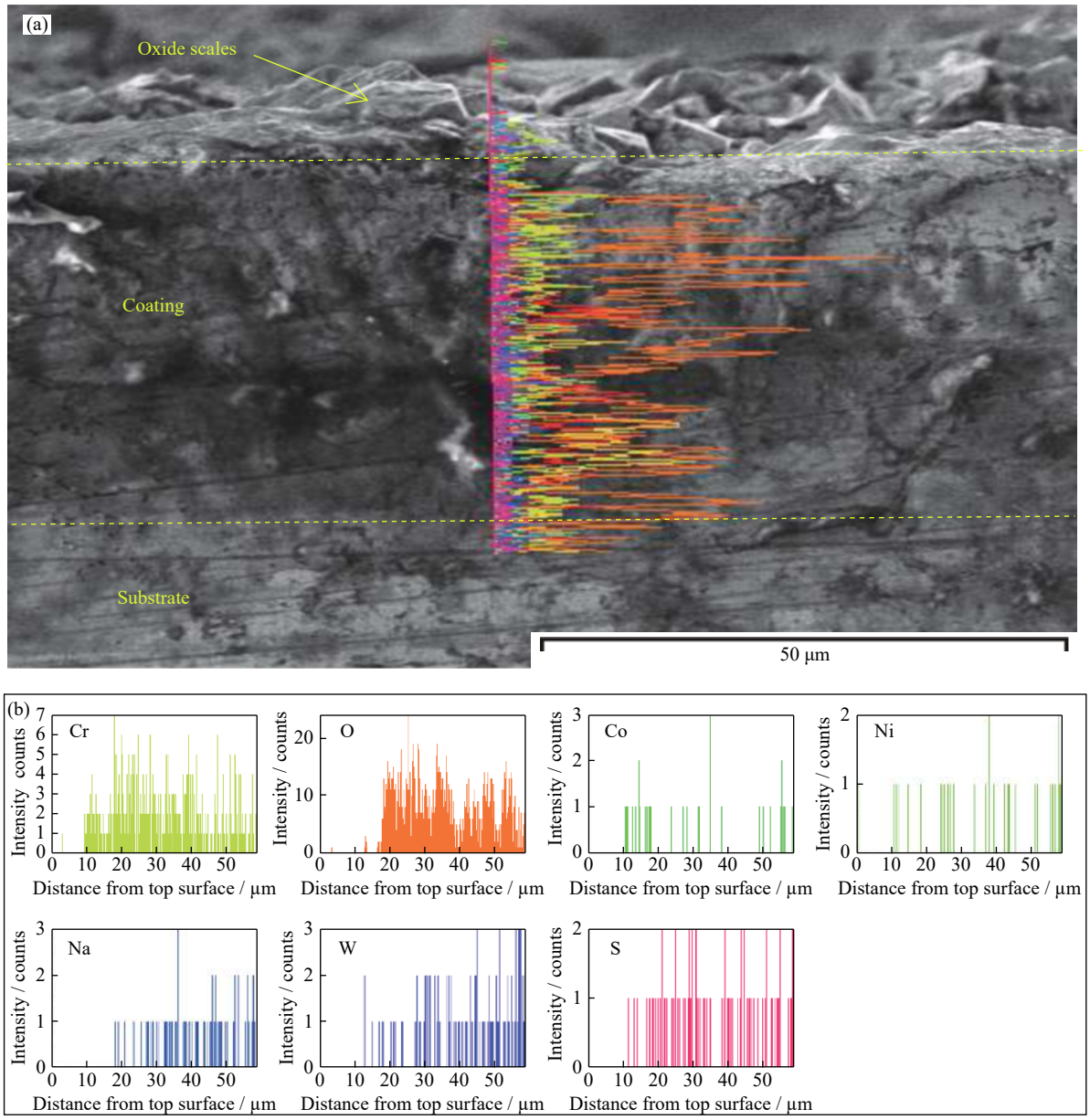

Fig. 13. Line mapping analysis for the cross section of the APS-coated L605 alloy subjected to hot corrosion after 50 cycles at 850°C: (a) mapping direction; (b) distribution of different elements.

corrosion cycles. The optical microscopic images and SEM images show less porosity and cracks in the HVOF-coated samples compared to the APS-coated and uncoated samples. The porosity of the coatings and the oxide layer formed during hot corrosion have a significant role in determining the comparative corrosion rate of the samples. The porosities and cracks in the coating will expose the alloy metal to a corroding environment, resulting in the formation of oxide layers and an increase in the corrosion rate. Due to the high-impact velocity of CoNiCrAlY powder coating by the HVOF process, a dense structure was achieved compared to the porous structure from APS. The porosity resulting from APS acts as an open pathway for corrosion, enabled corrosive elements to penetrate the substrate surface. Thus, the corrosion resistance of the HVOF-coated sample was better compared to that of the APS-coated sample. The thermogravimetric analysis of the samples shows that the HVOF-coated sample gained less weight compared to the APS-coated and uncoated samples; this is indicated in Fig. 7. The sequence of weight gain determined by corrosion rate after the 50th cycle was uncoated > APS-coated > HVOF-coated.

The HVOF coating offers the finest hot corrosion resistance to the L605 alloy. The weight gain measured after 50 cycles of hot corrosion for the HVOF-coated sample was 0.695 mg/cm^2, which was less than the weight gain value of 1.25 mg/cm^2 for the APS-coated sample. The uncoated

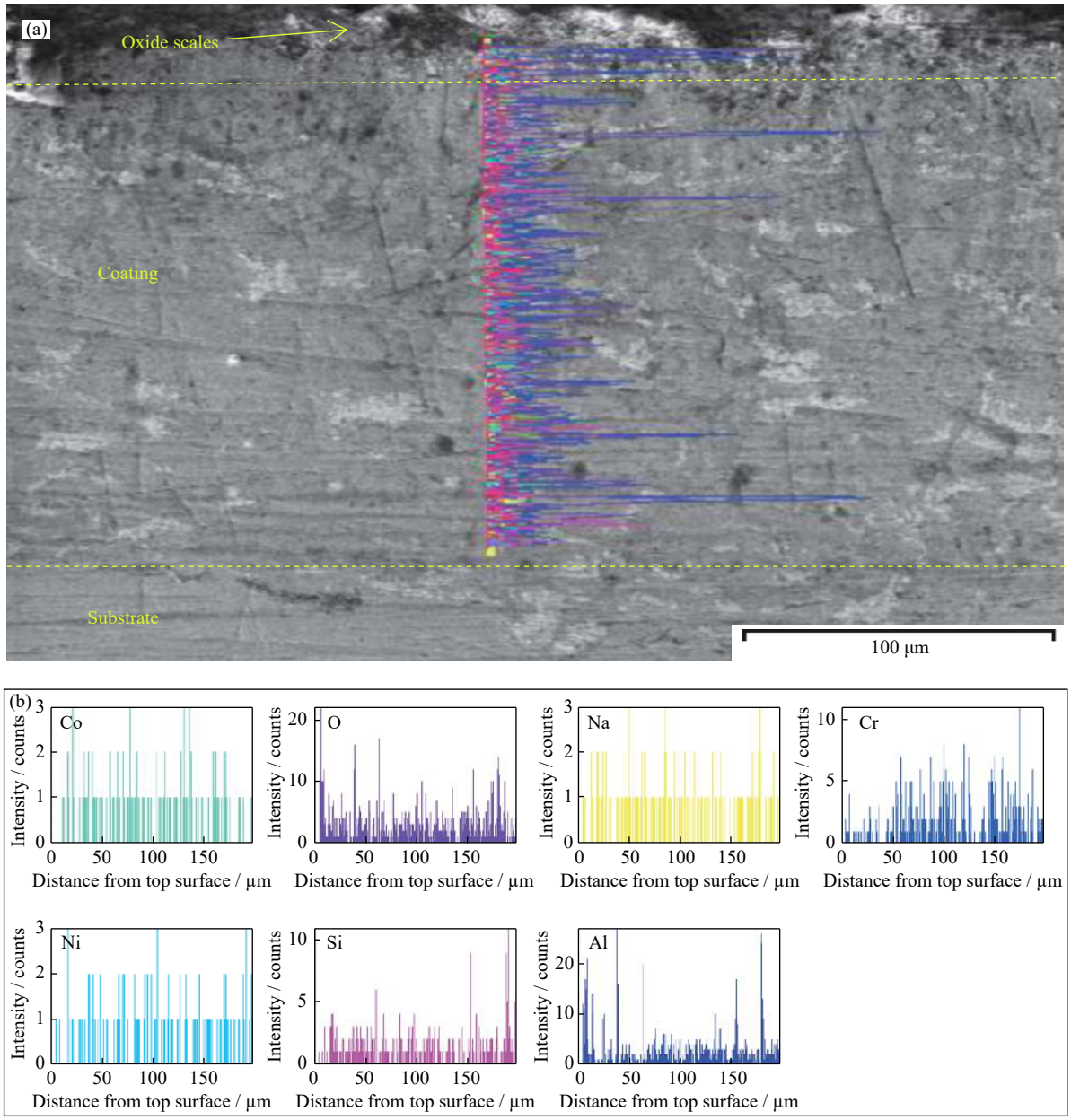

Fig. 14. Line mapping analysis for the cross section of the HVOF-coated L605 alloy subjected to hot corrosion after 50 cycles at 850°C: (a) mapping direction; (b) distribution of different elements.

sample had a weight gain of 4.87 mg/cm^2, which was much higher than the values of the coated samples. The weight gain of the APS- and HVOF-coated samples with respect to that of the uncoated sample was decreased by 74.3% and 85.7%, respectively. This was due to the poor corrosion resistance of the uncoated sample in the salt environment. There was a rapid increase in weight gain during the initial stages of the study for the coated samples of the L605 alloy; this was due to the quick formation of oxides on the coated surface during the inetial cycles. A protective oxide layer formed that covered all the surfaces and pores in the coatings, thus reducing internal oxidation. Once the oxide layer formed, it became stable and showed constant growth. This protective layer mainly consisted of Al_2O_3 and Cr_2O_3, derived from Al and Cr in the coating powder. This suppressed the hot corrosion of the coated samples in further cycles [18]. In the case of the uncoated sample, continuous growth of unprotective oxide layers occurred on the substrate surface owing to the accelerated corrosion resulting from the molten salt and elevated temperatures. When these non-protective oxide layers reach a critical thickness, sputtering, and spallation resulted.

Fig. 9 shows the surface SEM image of the uncoated sample, which shows oxide scales and porosities formed underneath the oxide scales because of the attack of the salt environment. The pores formed in the surface increased the diffusion rate, facilitating the molten salt to attack the substrate

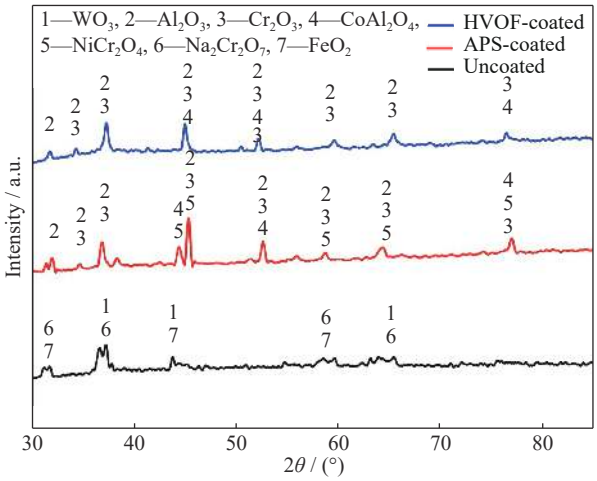

Fig. 15. XRD analysis of the uncoated, APS-coated, and HVOF-coated L605 alloy subjected to hot corrosion after 50 cycles at 850°C.

surface and thus increasing the corrosion rate of the sample. For the APS-coated sample, the SEM image shows that the coating surface had many oxidized areas of varying size and shape, which indicated the different rates of oxidation in different areas of the surface. This was due to the heterogeneous chemistry of the coating in the coated sample and the presence of pores and unmelted particles in the coating. The SEM images of the HVOF-coated sample revealed a dense structure with an uneven surface, and the image demonstrated proper adhesion of the coating to the substrate surface. This was achieved owing to the high-impact velocity of the HVOF coating method, making it a better technique compared to the APS coating method.

The EDS analysis shows the presence of O, W and Na in the oxide scale that formed on the surface of the uncoated sample. XRD analysis confirmed the presence of WO_3, $Na_2Cr_2O_7$, and FeO_2 in the uncoated samples. The presence of WO_3 and FeO_2 in the oxide scale indicated a high corrosion rate. The EDS analysis revealed a high amount of aluminum in the HVOF-coated sample compared to the APS-coated sample, and XRD analysis confirmed the presence of defensive oxide scales, such as Al_2O_3, Cr_2O_3, and $CoAl_2O_4$. The high thermal stability of the defensive oxides and yttrium content in the HVOF-coated sample provided better adhesion to the these oxides, giving the HVOF-coated sample a high corrosion resistance [4,18–20]. Additionally, the Al_2O_3 in the sample prevented internal oxidation, thus further aiding the corrosion resistance of the HVOF-coated sample.

5. Conclusions

A CoNiCrAlY coating was successfully coated to a L605 alloy via HVOF and APS coating processes, where the HVOF coating method was confirmed to have an excellent corrosion resistance compared to the APS coating method after 50 cycles of hot corrosion in a simulated gas turbine environment of 87.5wt% Na_2SO_4 + 7.5wt% $NaVO_3$ + 5wt% NaCl at 850°C.

(1) Owing to the high-impact velocity of the HVOF coating method, a dense coating with negligible porosity was achieved, which prevented diffusion of molten salt during hot corrosion and decreasing the susceptibility of the sample to corrosion.

(2) The presence of Na_2SO_4, $NaVO_3$, and NaCl led to severe deterioration of the uncoated sample. However, the APS- and HVOF-coated samples offered better protection in this environment. The SEM, EDS, and XRD results show that the HVOF-coated sample was rich with a protective oxide layer of Al_2O_3 and Cr_2O_3 after 50 cycles of hot corrosion, thus making it the least susceptible to hot corrosion.

(3) In coated samples, the formation of Al_2O_3 and Cr_2O_3 in the coating acts as a diffusion barrier that could resists the inward movement of the corrosive species present in the molten salt.

(4) Thermogravimetric analysis shows the weight gain determined by corrosion rate after the 50th cycle increased in the order of HVOF-coated L605 alloy, APS-coated L605 alloy, and uncoated L605 alloy.

(5) From the lower weight gain of HVOF-coated sample, we inferred that the HVOF sample was comparatively less corroded than the other samples and that the HVOF coating method helped decrease the corrosion rate of the L605 alloy.

References

[1] M. Gell, J.W. Wang, R. Kumar, J. Roth, C. Jiang, and E.H. Jordan, Higher temperature thermal barrier coatings with the combined use of yttrium aluminum garnet and the solution precursor plasma spray process, *J. Therm. Spray Technol.*, 27(2018), No. 4, p. 543.

[2] J. Stringer, High-temperature corrosion of superalloys, *Mater. Sci. Technol.*, 3(1987), No. 7, p. 482.

[3] N.R. Muktinutalapati, A. Natarajan, and M. Arivarasu, Hot corrosion of superalloys in boilers for ultra-supercritical power plants, [in] S. Cevik, eds., *Superalloys for Industry Applications*, IntechOpen, Croatia, 2018, p. 29.

[4] N. Jegadeeswaran, K. Udaya Bhat, and M.R. Ramesh, Improving hot corrosion resistance of cobalt based superalloy (Superco-605) using HVOF sprayed oxide alloy powder coating, *Trans. Indian Inst. Met.*, 68(2015), No. Suppl. 2, p. s309.

[5] N. Jegadeeswaran, M.R. Ramesh, S. Prakrathi, and K. Udaya Bhat, Hot corrosion behaviour of HVOF sprayed stellite-6 coatings on gas turbine alloys, *Trans. Indian Inst. Met.*, 67(2014), No. 1, p. 87.

[6] G.R. Heath, P. Heimgartner, G. Irons, R.D. Miller, and S. Gustafsson, An assessment of thermal spray coating technologies for high temperature corrosion protection, *Mater. Sci. Forum*, 251-254(1997), p. 809.

[7] M. Arivarasu, M. Venkatesh Kannan, K. Devendranath Ramkumar, and N. Arivazhagan, Hot-corrosion resistance of dissimilar AISI 4340 and AISI 304L weldments in the molten salt environment at 600°C, *Corros. Eng. Sci. Technol.*, 52(2017), No.

2, p. 114.

[8] H. Singh, Gitanjaly, S. Singh, and S. Prakash, High temperature corrosion behaviour of some Fe-, Co- and Ni-base superalloys in the presence of Y_2O_3 as inhibitor, *Appl. Surf. Sci.*, 255(2009), No. 15, p. 7062.

[9] J. Cizek and J. Matejicek, Medicine meets thermal spray technology: A review of patents, *J. Therm. Spray Technol.*, 27(2018), No. 8, p. 1251.

[10] T. Hussain, T. Dudziak, N.J. Simms, and J.R. Nicholls, Fireside corrosion behavior of HVOF and plasma-sprayed coatings in advanced coal/biomass co-fired power plants, *J. Therm. Spray Technol.*, 22(2013), No. 5, p. 797.

[11] N. Bala, H. Singh, S. Prakash, and J. Karthikeyan, Investigations on the behavior of HVOF and cold sprayed Ni–20Cr coating on T22 boiler steel in actual boiler environment, *J. Therm. Spray Technol.*, 21(2012), No. 1, p. 144.

[12] J.C. Tan, L. Looney, and M.S.J. Hashmi, Component repair using HVOF thermal spraying, *J. Mater. Process. Technol.*, 92-93(1999), p. 203.

[13] L.M. Sun, Thermal spray coatings on orthopedic devices: When and how the FDA reviews your coatings, *J. Therm. Spray Technol.*, 27(2018), No. 8, p. 1280.

[14] A. Mangla, V. Chawla, and G. Singh, Comparative study of hot corrosion behavior of HVOF and plasma sprayed Ni20Cr coating on SA213(T22) boiler steel in Na_2SO_4–60%V_2O_5 environment, *Int. J. Eng. Sci. Res. Technol.*, 6(2017), No. 10, p. 674.

[15] H. Singh, B.S. Sidhu, D. Puri, and S. Prakash, Use of plasma spray technology for deposition of high temperature oxidation/corrosion resistant coatings—A review, *Mater. Corros.*, 58(2007), No. 2, p. 92.

[16] V. Mannava, A.S. Rao, N. Paulose, M. Kamaraj, and R.S. Kottada, Hot corrosion studies on Ni-base superalloy at 650°C under marine-like environment conditions using three salt mixture (Na_2SO_4 + NaCl + $NaVO_3$), *Corros. Sci.*, 105(2016), p. 109.

[17] N.S. Patel, V. Pavlík, and M. Boča, High-temperature corrosion behavior of superalloys in molten salts—A review, *Crit. Rev. Solid State Mater. Sci.*, 42(2017), No. 1, p. 83.

[18] K. Zhang, M.M. Liu, S.L. Liu, C. Sun, and F.H. Wang, Hot corrosion behaviour of a cobalt-base super-alloy K40S with and without NiCrAlYSi coating, *Corros. Sci.*, 53(2011), No. 5, p. 1990.

[19] J.B. Yan, Y.M. Gao, L. Liang, Z.Z. Ye, Y.F. Li, W. Chen, and J.J. Zhang, Effect of yttrium on the cyclic oxidation behaviour of HP40 heat-resistant steel at 1373 K, *Corros. Sci.*, 53(2011), No. 1, p. 329.

[20] P. Choquet and R. Mevrel, Microstructure of alumina scales formed on NiCoCrAl alloys with and without yttrium, *Mater. Sci. Eng. A*, 120-121(1989), Part 1, p. 153.